The Meteoritical Society

Meteoritics & Planetary Science 51, Nr 6, 1003–1021 (2016)
doi: 10.1111/maps.12644

Aqueous alteration of chondrules from the Murchison CM carbonaceous chondrite: Replacement, pore filling, and the genesis of polyhedral serpentine

M. R. LEE* and P. LINDGREN

School of Geographical and Earth Sciences, University of Glasgow, Glasgow G12 8QQ, UK
*Corresponding author. E-mail: martin.lee@glasgow.ac.uk

(Received 24 June 2015; revision accepted 24 February 2016)

Abstract–Forsterite and clinoenstatite in type IAB chondrules from the Murchison CM carbonaceous chondrite have been partially serpentinized, and the mechanisms of their alteration reveal crystallographic and microstructural controls on the reaction of silicate minerals with parent body aqueous solutions. Grains of forsterite were altered in two stages. Narrow veinlets of Fe-rich serpentine formed first and by the filling of sheet pores. Most of these pores were oriented parallel to (010) and (001) and had been produced by earlier fracturing and/or congruent dissolution. In the second stage, the subset of veinlets that were oriented parallel to (001) was widened accompanying the replacement of forsterite by Mg-Fe serpentine. This reaction proceeded most rapidly parallel to [001], and crystallographic controls on the trajectory of retreating vein walls created fine-scale serrations. Murchison clinoenstatite grains have a skeletal appearance due to the presence of abundant veinlets and patches of phyllosilicate. Two alteration stages can again be recognized, with initial water–mineral interaction producing tochilinite-rich veinlets by the filling of (001)-parallel contraction cracks. Pores then formed by congruent dissolution that was guided principally by orthopyroxene lamellae, and they were subsequently filled by submicrometer-sized crystals of polyhedral serpentine. This finding that Murchison forsterite and clinoenstatite grains have been altered demonstrates that aqueous processing of magnesium silicate minerals started much earlier in CM parent body history than previously believed. Our results also show that the occurrence of polyhedral serpentine can be used to locate former pore spaces within the parent body.

INTRODUCTION

The occurrence within CM carbonaceous chondrite meteorites of minerals including phyllosilicates and carbonates is good evidence for the former presence of liquid water in the interiors of their parent body(ies) (e.g., DuFresne and Anders 1962; McSween 1979; Bunch and Chang 1980; Browning et al. 1996). These secondary minerals formed within a few million years of the earliest solar system solids (Endress et al. 1996; Hutcheon et al. 1999; Brearley and Hutcheon 2002; De Leuw et al. 2009; Fujiya et al. 2012; Lee et al. 2012) and by the alteration of primary anhydrous constituents such as Fe, Ni metal and Fe-sulfides, silicate minerals, and amorphous materials (e.g., Bunch and Chang 1980; Barber 1981, 1985; Richardson 1981; Tomeoka and Buseck 1985; Zolensky et al. 1993; Greenwood et al. 1994; Lee and Greenwood 1994; Browning et al. 1996; Chizmadia and Brearley 2008; Howard et al. 2009, 2011; Velbel et al. 2012, 2015). The extent of alteration differs between CM meteorites and ranges from partial to complete (e.g., Zolensky et al. 1997; Rubin et al. 2007). The most highly reactive of the primary constituents was amorphous materials (including chondrule mesostasis glass) and melilite, which are preserved only in the least altered meteorites (e.g., Y 791198, Paris, EET 96029) (Chizmadia and Brearley 2008; Hewins et al. 2014; Lindgren et al. 2015). Olivine, clinopyroxene, and orthopyroxene were less reactive and so are present in all but the most highly aqueously processed CMs, which are classified as "CM1" (Zolensky et al. 1997) or "CM2.0" (Rubin et al. 2007).

As a consequence of their occurrence within the majority of CMs, these silicate minerals can be used to explore the nature of the parent body aqueous system. For example, the extent of preservation of chondrule olivine has been used as a proxy for the relative degree of aqueous alteration (Browning et al. 1996; Rubin et al. 2007), and the chemical composition of serpentine that has formed by replacement of olivine has provided important new information into the length scale of the aqueous system (Hanowski and Brearley 2001; Velbel et al. 2012, 2015).

Despite the clear utility of chondrule silicates as tracers of parent body aqueous processing, surprisingly little is known about the drivers of their alteration (Velbel et al. 2015). Nonetheless, an understanding of the influence of mineral chemistry, crystal structure, and microstructure on alteration reactions has the potential to provide new insights into the nature and availability of aqueous solutions and the prealteration history of the CM parent body(ies). One question that can potentially be answered using chondrule silicates is whether early shock deformation catalyzed or enhanced alteration (Hanna et al. 2012; Rubin 2012; Lindgren et al. 2015). For example, the creation of fractures, dislocation networks, and subgrain boundaries may have served to accelerate rates of dissolution and replacement. Differences in the nature and extent of alteration of mineral pairs within individual chondrules can also be used to explore water–rock interaction. For example, Hanowski and Brearley (2001) found that olivine and clinoenstatite in ALH 81002 chondrules were more susceptible to aqueous processing than orthopyroxene and augite, and displayed contrasting styles of alteration. They showed that olivine has altered along fractures to produce serpentine veins, whereas clinoenstatite has a micropore-rich or "skeletal" appearance. Velbel et al. (2012, 2015) drew parallels between the textures of partially serpentinized olivine grains in chondrules from the CMs Nogoya and QUE 93005 and olivine in terrestrial basalts and serpentinites. However, they also noted that "the interface between olivine and serpentine is smooth and regular and lacks any orderly etching or denticulation textures (such as those common for terrestrial aqueous weathering of olivine)" (Velbel et al. 2015, p. 122). Thus, the apparent absence of serrations (i.e., denticulate textures) on vein walls, which would otherwise be indicative of olivine dissolution, questions whether olivine-hosted serpentine has formed by the same style of replacement as is commonplace on Earth.

Here, we report results of a petrographic and microstructural study of the aqueous alteration of forsteritic olivine and clinopyroxene from partially serpentinized chondrules in the Murchison CM carbonaceous chondrite. This meteorite has been selected because its chondrules have been less highly altered than those in the most other CM meteorites (e.g., Hanowski and Brearley 2001; Rubin et al. 2007). Thus, chondrule olivine and clinopyroxene grains may record the earliest stages of water–mineral interaction when any crystallographic and microstructural controls will be most easy to recognize. We hypothesize that intracrystalline determinants of aqueous alteration will be revealed by the crystallographic orientations of serpentine veins, the microstructures of their walls, and the internal structure of the vein fill. The broader context of this study is that olivine is an important tracer of the presence and longevity of liquid water on both Earth and Mars owing to its high reactivity in the presence of aqueous solutions (Stopar et al. 2006; Olsen and Rimstidt 2007; Velbel 2009). Thus, a better understanding of how olivine is altered by CM parent body aqueous solutions can also help to reveal the drivers of water–mineral interactions in terrestrial and Martian contexts.

MATERIALS AND METHODS

The Murchison CM carbonaceous chondrite fell in Australia in 1969, and more than 100 kg was recovered (Lovering and Le Maitre 1971; Graham et al. 1985). Most of the observations described herein are of polished block BM1970,5 (P19262), which was loaned by the Natural History Museum (London). In order to assess how representative this sample is of the Murchison meteorite, four other polished blocks were examined by SEM (Table 1). Each of the five samples was studied by backscattered electron (BSE) imaging using one of two field-emission SEMs, a FEI Quanta and a Zeiss Sigma. Both instruments were operated at 20 kV and in low vacuum mode as the blocks were initially uncoated. Contrast in the BSE images is largely a function of differences within the scanned area of mean atomic number (Z). The widths of serpentine veins were measured from these images, and values quoted are the maximum width taken parallel to [001] or [010], depending on whether the axis of the vein is parallel to (001) or (010), respectively.

All subsequent analytical work used BM1970,5 (P19262), and the objects that were studied in detail are listed in Table 2. In preparation for electron backscatter diffraction (EBSD), the uncoated block was briefly repolished in colloidal silica. EBSD was used to determine the crystallographic orientations of olivine and clinoenstatite (CEN) grains and features within them (e.g., fractures and veins). EBSD maps were acquired using an EDAX/TSL system attached to the Quanta SEM, which was operated at low vacuum and using a high beam current (which is not quantified on

Table 1. The proportion of type IAB chondrules in each of the five Murchison samples that contain partly serpentinized forsterite phenocrysts.

Murchison sample	Proportion of chondrules whose forsterite crystals host serpentine veins
BM1970,5 (P19262)	90%
BM1970,6 (P19258)	70%
BM1970,6 (P19259)	60%
BM1988,M23 (P19260)	50%
BM1988,M23 (P19261)	40%

Ten chondrules in each sample were examined by SEM. A chondrule is counted as containing partially serpentinized forsterite phenocrysts if at least one out of the five olivine grains that were examined host one or more veins.

Table 2. Summary of the work undertaken on Murchison sample BM1970,5 (P19262).

Object studied	Descriptor	Techniques used	Illustration
Type IA/IAB chondrule fragment	Coarse phenocryst	SEM, EBSD, TEM	Fig. 1
Type IAB chondrule	Chondrule 7	SEM, EBSD	Fig. 2
Type IAB chondrule	Chondrule 1	SEM, EBSD, TEM	Fig. 3
Type IAB chondrule	Chondrule 3	SEM, EBSD, TEM	Figs. 4–7

this SEM). Entire grains or parts of them were mapped at a submicrometer step size. Kikuchi patterns were indexed using structure files for forsterite (Fo_{92}) in the TSL database (a = 0.4762 nm; b = 1.0225 nm; c = 0.5994 nm), and this file is appropriate given that all of the olivine grains mapped were close to end-member forsterite (Fo) in chemical composition. The structure file for clinoenstatite was generated using unit-cell parameters in Ohashi (1984): a = 0.9606 nm; b = 0.88131 nm; c = 0.517 nm; β = 108.35°. Crystallographic orientations as determined by EBSD are here plotted as upper hemisphere pole figures. With regard to the olivine grains, several different poles, such as (100), (010), and (001), have been overlain to make a single composite figure, and the clusters of points that represent each pole are shown schematically. EBSD results from clinoenstatite are expressed as image quality maps and inverse pole figure maps in addition to pole figures. Contrast in the image quality maps represents differences over the mapped area in the quality of the Kikuchi pattern (e.g., sharpness of the Kikuchi bands). Results are provided in grayscale, with points that yield very poor patterns (e.g., holes) being black, whereas those that give good patterns are white. The inverse pole figure maps use color to represent the pole to the lattice plane that lies parallel to a selected reference direction. In the clinoenstatite pole figures, the actual points derived from the maps are plotted to show crystallographic orientations. The accuracy of the orientation data that were obtained by EBSD was double checked by acquiring transmission electron microscope (TEM) electron diffraction patterns from foils that had been cut from the same olivine and clinoenstatite grains using the FIB technique (see below). These tests confirm that the EBSD results are accurate.

Qualitative X-ray microanalysis and X-ray mapping were undertaken after carbon coating of the polished block and using the Zeiss Sigma SEM operated in high vacuum. Data were collected using an Oxford Instruments X-Max silicon-drift energy-dispersive X-ray detector that was operated through Aztec microanalysis software. The analyses were undertaken using a probe current of ~2 nA, and maps were acquired at a resolution of 1024 × 768 pixels. Five electron-transparent samples for TEM work were cut from the surface of the coated polished block using the focused ion beam (FIB) technique and following the procedure of Lee et al. (2003). Three of these foils were extracted from olivine grains and two from clinopyroxene grains (Table 3). Foils were prepared using a FEI DualBeam® instrument, which employs a Ga^+ ion beam for milling and an electron beam from a field-emission tip for imaging and deposition of protective platinum. Milling was undertaken at 30 kV and using a range of beam currents. After milling to ~1 μm thickness, each foil was removed from the polished block using an in situ micromanipulator and welded to the tines of a copper support grid. The foils were then milled further to a thickness of ~100 nm. Initial characterization of the foils used the low voltage scanning transmission electron microscopy technique (LV-STEM; Lee and Smith 2006) on the Zeiss SEM, operated at 20 kV/0.5 nA. In addition to bright- and dark-field imaging, qualitative chemical analysis was undertaken by LV-STEM and using the Oxford Instruments microanalysis system. Note that all of these X-ray spectra contain a substantial Al K_α peak that is derived from the sample holder, and this peak has been stripped from the figured spectra so that it is not misinterpreted as representing Al in the sample. Analysis of grains in the bulk sample by SEM-EDX indicates that the phyllosilicates that are the subject of this article are Al-poor, and so stripping of Al K_α peaks from the LV-STEM spectra will not change our interpretation. Bright-field and high-resolution TEM images, and selected area electron diffraction (SAED) patterns, were obtained from the foils using a FEI T20 instrument operated at 200 kV.

Table 3. Details of the foils extracted from Murchison sample BM1970,5 (P19262) for TEM work.

Descriptor	Foil reference (X-Y size)	Constituents	Approximate orientation of the foil midplane	Illustration
Coarse phenocryst	CP-foil A (8.6 × 3.2 μm)	Forsterite	$(110)_{Fo}$	Not shown
Coarse phenocryst	CP-foil B (10.4 × 4.9 μm)	Forsterite, serpentine	$(110)_{Fo}$	Fig. 1d
Chondrule 1	C1-foil A (10.2 × 6.9 μm)	Forsterite, serpentine	$(101)_{Fo}$	Fig. 3f
Chondrule 3	C3-foil A (14.0 × 7.5 μm)	Clinoenstatite, polyhedral serpentine, tochilinite	$(001)_{CEN}$	Fig. 6b
Chondrule 3	C3-foil B (9.9 × 5.3 μm)	Clinoenstatite, polyhedral serpentine, phyllosilicate	$(001)_{CEN}$	Figs. 7c–f

SAED patterns were manually indexed and using d-spacings and interplanar angles calculated from the same unit-cell parameters for forsterite and clinoenstatite as are quoted above. With regard to using EBSD and TEM-SAED to determine the crystallographic orientation of a feature such as serpentine vein, in most cases its orientation in three dimensions will be unknown. Thus, the feature is described as being oriented parallel to the "trace" of a given lattice plane or set of planes.

MINERALOGY OF MURCHISON

The modal mineralogy of Murchison, as determined by light microscopy and X-ray diffraction (XRD), is given in Table 4. Phyllosilicates are the main constituent of the fine-grained matrix of Murchison (and all other CM carbonaceous chondrites) and have formed by parent body aqueous alteration. The mineralogy and chemical composition of Murchison has been used in various ways over the last 20 years to show that it is one of the least aqueously altered CMs available for study. Browning et al. (1996) classified seven CMs according to their "Mineralogical Alteration Index" and found that Murchison was the least altered meteorite in their sample set. Rubin et al. (2007) examined 11 CMs and gave each a subtype, using a suite of mineralogical and chemical criteria, which ranged from CM2.6 (least altered) to CM2.0 (most highly altered). Murchison was a CM2.5, thus making it the least altered bar one of the 11 meteorites. Howard et al. (2015) ranked 25 CMs according to their normalized fraction of phyllosilicates as determined by XRD. The phyllosilicate fraction increases with a greater degree of alteration so that a type 3.0 meteorite would have a phyllosilicate fraction of <0.05 and type 1.0 meteorite would have a phyllosilicate fraction of >0.95. The 25 CMs ranged from types 1.7 to 1.2, with Murchison classified as type 1.5. Only 3 of the other 24 meteorites were more highly altered. Alexander et al. (2013) classified 54 CMs according to the weight percent of H in water and OH. This index reflects the degree of hydration (i.e., the aqueous alteration of anhydrous components to phyllosilicates), but is also affected by the loss of H during subsequent heating. The scale extends from 1 (most hydrated) to 3 (least hydrated). Murchison is classified as a 1.6, and 17 of the CMs were less highly hydrated (i.e., >1.6). When related to its bulk hydrogen isotope composition, the classification of 1.6 also indicates that Murchison was not heated after aqueous alteration to a level sufficient to drive off water or hydroxyls (Alexander et al. 2013).

Murchison is unshocked (it has a shock stage of S1: Scott et al. 1992; Tomeoka et al. 1999; Rubin 2012), although Hanna et al. (2012) and Lindgren et al. (2015) have shown that at least some parts of the meteorite display a petrofabric as a consequence of having experienced multiple low-intensity impacts. The five samples studied here show no evidence for terrestrial weathering during their 45 years of museum storage.

RESULTS

The focus of this study is on the serpentinization of olivine and clinopyroxene within type IAB chondrules and chondrule fragments, and in these objects, the two minerals have close to end-member chemical compositions (i.e., forsterite and enstatite) (Lovering and Le Maitre 1971; Fuchs et al. 1973). Grains of augite and orthopyroxene also occur in type IAB chondrules, but as they are unaltered in the samples studied, these two minerals are not considered further. Our work has concentrated on BM1970,5 (P19262), within which 9 of the 10 type IAB chondrules that were examined by SEM contain forsterite phenocrysts with serpentine veins (Table 1). In order to assess how representative the degree of alteration of BM1970,5 (P19262) is of Murchison more broadly, the proportion of type IAB chondrules that contain partially serpentinized forsterite grains was determined in four other polished blocks of the same meteorite (Table 1). The results show that BM1970,5 (P19262) contains the highest proportion of chondrules with altered forsterite.

Table 4. Modal mineralogy of Murchison.

	Vol%
McSween (1979), using light microscopy	
Matrix	63.6
Chondrules and polymineralic fragments	16.1
Monomineralic grains and fragments	11.4
Amoeboid olivine and Ca- and Al-rich inclusions	8.3
Opaque minerals	0.6
Howard et al. (2011), using X-ray diffraction	
Phyllosilicates (Fe-cronstedtite and Mg-serpentine)	72.5
Olivine and orthopyroxene	23.4
Sulfide	1.8
Calcite	1.2
Magnetite	1.1

Partially serpentinized grains of forsterite and clinopyroxene were studied in detail where they occur together within three porphyritic type IAB chondrules (chondrules 1, 3, and 7; Table 2). The analytical techniques that were used to characterize these chondrules are also listed in Table 2. We additionally used SEM, EBSD, and TEM to study a partially serpentinized forsterite phenocryst that is the main constituent of a single fragment of a porphyritic type IA/type IAB chondrule. This object is hereafter referred to as the "coarse phenocryst" (Table 2).

The descriptions below recognize two varieties of phyllosilicate veins within forsterite, which are distinguished by differences in their width and crystallographic orientation (1) submicrometer wide "high-Z veinlets," whose axes are close to the trace of $(010)_{Fo}$ (i.e., normal to $[010]_{Fo}$, the forsterite *b* axis); (2) "serpentine veins," which are a few micrometers in width, and whose axes lie near parallel to the trace of $(001)_{Fo}$ (i.e., normal to $[001]_{Fo}$, the forsterite *c* axis). The high-Z veinlets and serpentine veins either crosscut entire olivine grains or are described as being "discontinuous" (i.e., they terminate within grains).

Coarse Phenocryst

This forsterite phenocryst is 221 μm in width and contains ten serpentine veins, eight of which are discontinuous (Fig. 1a). The axes of these veins lie parallel or at a low angle (<25°) to the trace of $(001)_{Fo}$, as measured by both EBSD and TEM-SAED. The veins are 5.6–9.6 μm in width (mean = 7.1 μm, $n = 10$ veins). Their walls are straight or gently curving, and some are serrated (Figs. 1b and 1c). The vein fill contains bands that differ significantly in Z (Figs. 1b–d). Most veins have a narrow and parallel-sided axial band that commonly has a relatively high Z (Fig. 1b). Flanking bands are wider, they often have a lower Z, and their mutual boundaries are commonly serrated with teeth and notches being oriented parallel to the traces of $\{111\}_{Fo}$. The vein fill is finely crystalline (Fig. 1d), and SAED patterns yield d-spacings of ~0.7 nm, which is consistent with serpentine. The structure of the patterns shows that phyllosilicate crystals within the high-Z bands are coarser than those in the lower Z bands, and oriented with their *c* axes normal to the vein axis (i.e., parallel to $[001]_{Fo}$). The phyllosilicates are rich in O, Mg, Si, and Fe, but may also contain S and Ni (Figs. 1e and 1f). Bands with the highest Z have the greatest concentrations of S, Fe, and Ni (Fig. 1f). TEM images of a foil that was cut from just beyond the tip of the discontinuous vein in Fig. 1b (CP-foil A) show that the host forsterite lacks subgrain boundaries and is free of defects (i.e., it has a dislocation density of $<10^6$ cm^{-2}).

Type IAB Chondrules

Grains of forsterite in the three chondrules that were studied in detail are euhedral or subhedral, ~15–80 μm in size, and their long axes are typically parallel to $[001]_{Fo}$. They commonly contain ~1- to 6-μm-sized spherules of Fe, Ni metal and patches of high-Z alteration products of the same size and shape. Clinoenstatite occurs as lath-shaped grains, up to ~100 μm in size, which are elongate parallel to $[001]_{CEN}$. Where not in contact with other silicate minerals, the forsterite and clinopyroxene grains are enclosed by phyllosilicate-rich mesostasis (e.g., Fig. 2a).

Olivine-Hosted Serpentine Veins and High-Z Veinlets

Almost all of the forsterite grains in chondrules 1, 3, and 7 contain serpentine veins. Any one grain has between one and three veins whose axes lie parallel or at a low angle to the trace of $(001)_{Fo}$ (Figs. 2 and 3). They are 2.9–5.8 μm in width (mean = 4.1 μm, $n = 8$ veins in four grains), and most veins crosscut the whole of their host grain (Figs. 2a, 2b, and 3c–e). Vein walls are commonly serrated; the teeth and notches typically have a wavelength of 1.7–2.8 μm and an amplitude of 0.6–1.2 μm (Figs. 2a, 2b, and 3c–e). The amplitude is greatest (i.e., the teeth and notches are most pronounced) in those grains whose polished surface lies close to the trace of $(100)_{Fo}$ (e.g., Fig. 2a). Some forsterite grains host veins whose walls have teeth and notches with an unusually high amplitude relative to their wavelength (Fig. 2b). Veins may also be curved, and as their axes progressively depart from the trace of $(001)_{Fo}$, they narrow and occasionally pinch out, and their walls lose serrations (Figs. 2b and 3d).

Vein fills have a common internal structure comprising a high-Z axial band that is straight and a

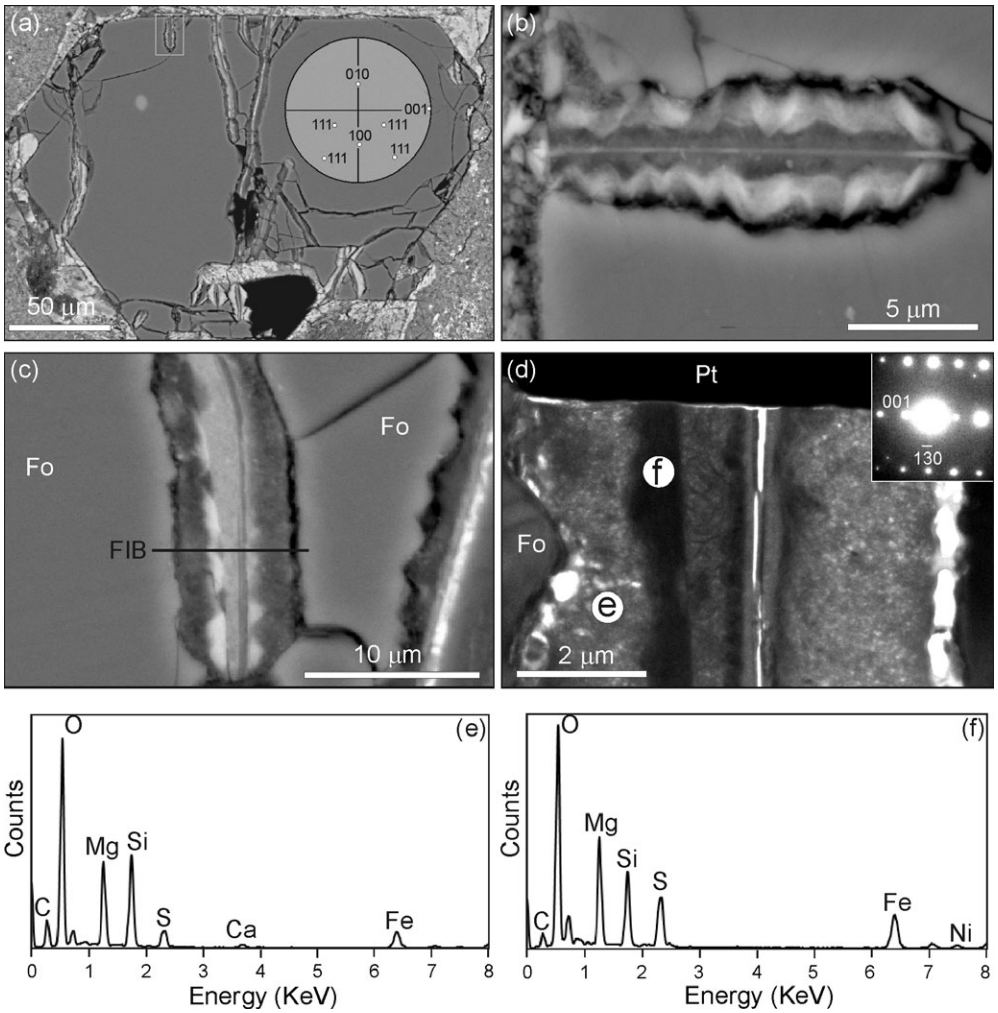

Fig. 1. Serpentine veins within the "coarse phenocryst" chondrule fragment. a) BSE image of the euhedral forsterite phenocryst whose serpentine veins are highlighted by high-Z (i.e., white) bands within their fill. The inset EBSD pole figure shows that vein axes lie parallel or at a low angle to the trace of $(001)_{Fo}$. b) BSE image of the discontinuous vein in the top left of the phenocryst (highlighted by the boxed area in [a], and note that it has been rotated 90° anticlockwise relative to [a]). The vein has a very narrow and straight high-Z axial band, which is flanked by several bands that are distinguished by differences in Z. Contacts between these flanking bands are serrated, and EBSD shows that the serrations are parallel to the traces of $\{111\}_{Fo}$. c) BSE image of a vein that contains high-Z bands with serrated outer edges. d) Bright-field TEM image of foil (CP-foil B) that was extracted from the vein in (c), and whose midplane is indicated by the black line in (c) labeled "FIB." The serpentine is finely crystalline, and differences in its grayscale reflect contrasts in Z (i.e., the black bands have a high Z and so attenuate electrons most effectively). Note the forsterite tooth projecting from the left hand side vein wall. The inset $[310]_{Fo}$ SAED pattern shows that the vein axis is parallel to the trace of $(001)_{Fo}$. White areas are fractures in the foil, and Pt denotes the FIB-deposited platinum strap. (e) and (f) are LV-STEM X-ray spectra obtained from the points in (d) that are labeled e and f, respectively.

few hundred nanometers in width and is flanked by one or more bands with a lower Z (Figs. 2a, 2b, and 3c–f). This fill is dominated by O, Mg, Si, and Fe, and high-resolution TEM shows that the constituent crystals have a ~0.7 nm lattice fringe spacing that is consistent with serpentine. The high-Z axial bands are enriched relative to flanking bands with respect to Fe and also often contain S. The interfaces between flanking bands are commonly serrated (Fig. 2a). The high-Z band may extend beyond the olivine grain and into the mesostasis, where it forms a narrow curving vein (Fig. 3e). Forsterite grains may also contain open fractures that have a range of crystallographic orientations (Fig. 2b), and some of them intersect serpentine veins. In a few cases, the serpentine extends for a several micrometers into the otherwise open fracture, thus showing that the fracture was present during formation of the vein fill.

In addition to the veins, most forsterite grains contain one or two of the narrow high-Z veinlets, whose axes lie close the trace of $(010)_{Fo}$ (Figs. 2b, 3c, and 3d).

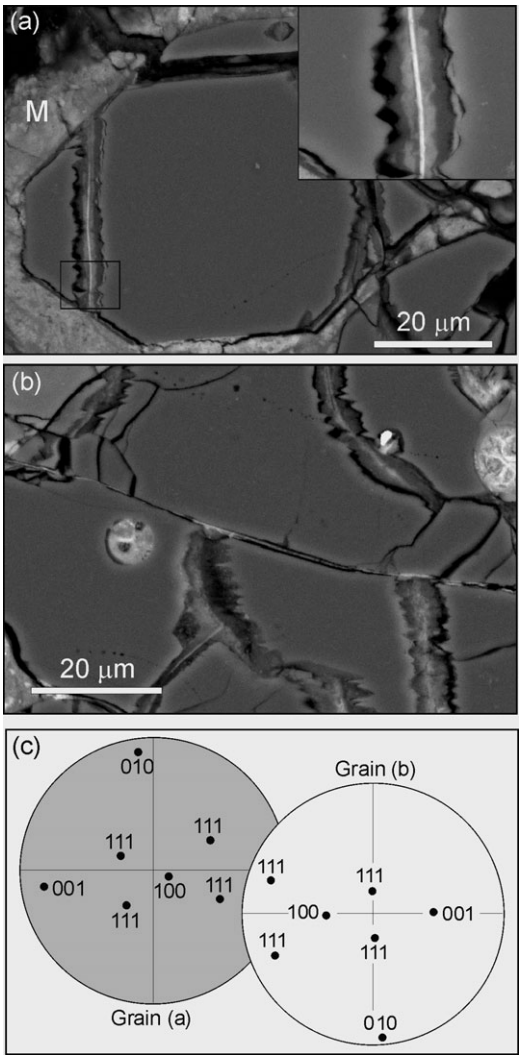

Fig. 2. (a) and (b) are BSE images of forsterite grains in chondrule 7. EBSD pole figures showing the crystallographic orientations of these grains are in (c). The grain in (a) contains two serpentine veins, whose axes are parallel to the trace of $(001)_{Fo}$. A veinlet close to the upper margin of the grain is parallel to the trace of $(010)_{Fo}$. The veins have serrated walls, and part of the left hand side vein is shown enlarged in the inset (top right). The fill of this vein comprises a narrow and straight high-Z axial band, which is flanked by two bands of lower Z, and the interfaces between these flanking bands are serrated. The three widest serpentine veins in (b) are oriented with their axes approximately parallel to the trace of $(001)_{Fo}$, and the serrations on their walls have an unusually high amplitude relative to their wavelength. The vein in the upper right-hand side of the grain curves downwards, and away from the trace of $(001)_{Fo}$. As it curves, the vein walls lose their serrations. The two veins in the lower part of the grain both terminate against a narrow high-Z veinlet whose axis lies at a low angle to the trace of $(010)_{Fo}$ and whose walls lack serrations.

These veinlets are typically ~100–400 nm in thickness and parallel sided, and so they are very similar in appearance to the axial bands of the wider and $(001)_{Fo}$-parallel serpentine veins. The high-Z veinlets can be traced into the mesostasis, where they are sinuous and sometimes also branching, and may occasionally join with the high-Z axial band of a serpentine vein in the same grain (Fig. 3e). The $(001)_{Fo}$-parallel serpentine veins terminate abruptly where they meet veinlets (Figs. 2b, 3d, and 3e).

The margins of those grains that are enclosed by the mesostasis are commonly lined by a selvage of serpentine. These selvages were referred to as "chondrule silicate rims" by Browning et al. (2000) and "alteration rinds" or "centripetal replacement shells" by Velbel et al. (2015); here, we use the latter term. Centripetal replacement shells are widest on those grain margins that are parallel to the trace of $(001)_{Fo}$, and the interface between the serpentine and olivine is often finely serrated (Fig. 3c). The shells thin and then pinch out as grain margins curve away from $(001)_{Fo}$ and are absent from those margins that are parallel to the traces of $(100)_{Fo}$ and $(010)_{Fo}$ (Fig. 3c).

Clinoenstatite Microstructure and Alteration Products

Clinoenstatite grains in chondrules 1, 3, and 7 have ~1–5 μm thick twins that are oriented parallel to the trace of $(100)_{CEN}$ (and so also parallel to the long edges of these lath-shaped grains) (Fig. 4). Both of the grains in chondrule 3 that were examined by TEM additionally contain closely spaced lamellae of orthopyroxene, which also lie parallel to the trace of $(100)_{CEN}$.

The skeletal appearance that characterizes all of the clinoenstatite grains in chondrules 1, 3, and 7 is due to the presence of veinlets and patches of secondary minerals (Fig. 4a). The veinlets are ~0.6–2.8 μm in width and ~3–30 μm in length. They are usually discontinuous, and oriented parallel to the trace of $(001)_{CEN}$, or less commonly parallel to the trace of $(100)_{CEN}$ (Figs. 4 and 5b–d). The veinlets are distinguished from phyllosilicate patches by the higher Z of their fill and the common occurrence within them of high-Z fibers (Figs. 5b–d and 6). LV-STEM X-ray spectra show that the veinlets are rich in O, S, and Fe, with lower concentrations of Mg, Si, and Ni (Fig. 6c). TEM imaging reveals the presence of corrugated laths with a lattice fringe spacing of ~1.08 nm or ~0.54 nm. The high-Z fill of the veinlets is, therefore, comparable in chemical composition and structure to Fe-rich tochilinite, which has the formula $6Fe_{0.9}S$ 5(Fe, Mg) $(OH)_2$ (Mackinnon and Zolensky 1984). This mineral is formed from a coherent interstratification of mackinawite and brucite sheets, and its d-spacings include 1.084 and 0.541 nm (Mackinnon and Zolensky 1984).

Phyllosilicate patches range from rectilinear to irregular in shape (Figs. 5 and 7). Rectilinear patches

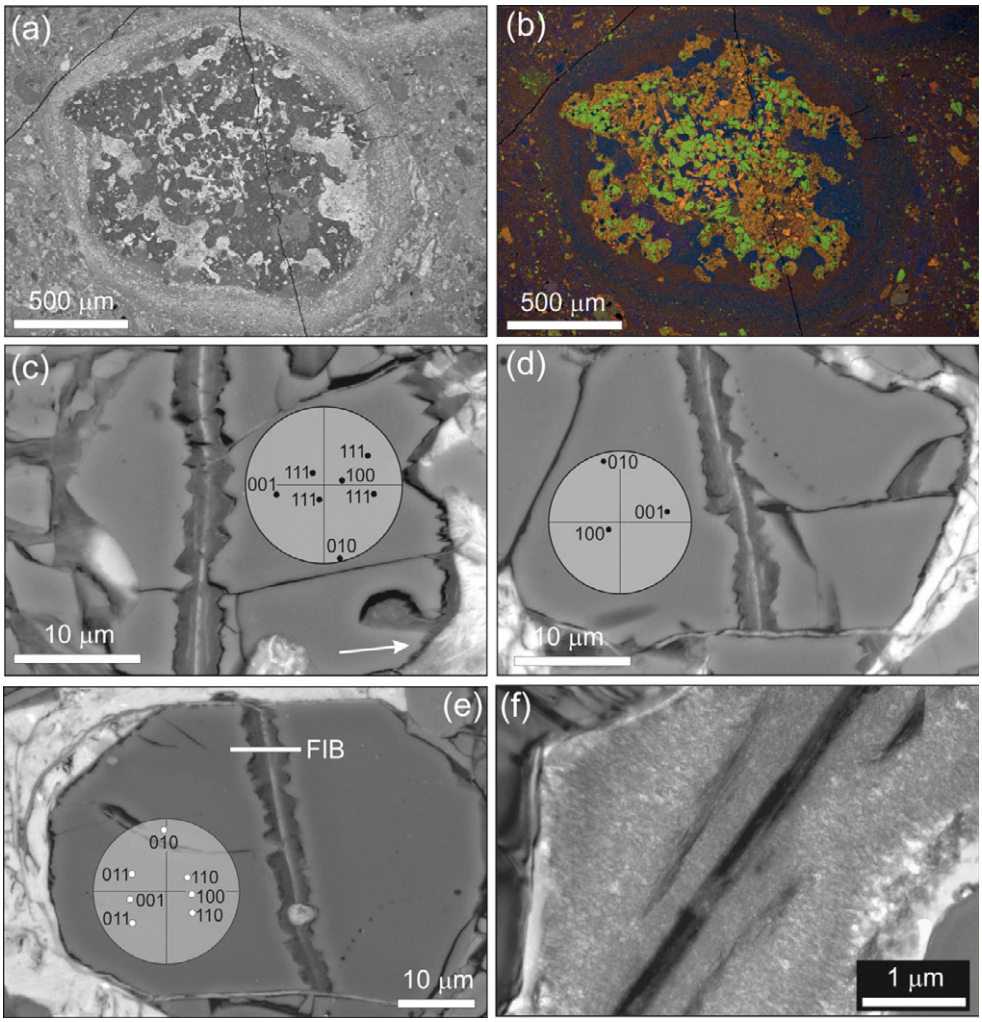

Fig. 3. Images of chondrule 1 and its forsterite grains. a) BSE image of the chondrule, which is enclosed by a fine-grained rim. b) X-ray map of (a) that has been made by blending four elements: Mg (light green), Si (purple), Ca (yellow), and Fe (light blue). Forsterite is light green, clinoenstatite is dark orange, augite is light orange, and the blue areas are S-bearing Fe-rich oxides. (c)–(e) are BSE images of forsterite grains whose crystallographic orientations are shown by the inset EBSD pole figures. c) A grain that hosts a $(001)_{Fo}$-parallel serpentine vein that has a high-Z axial band and serrated walls. The grain also contains two narrow high-Z veinlets whose axes are close to the trace of $(010)_{Fo}$. The right-hand margin of the grain has a centripetal replacement rim, which is distinguished from the mesostasis by its considerably lower Z. Forsterite abutting this rim has fine-scale serrations. The rim thins as the grain margin curves away from $(001)_{Fo}$ (arrowed). d) A grain that is bisected by a $(001)_{Fo}$-parallel serpentine vein with serrated walls. Close to the right-hand margin of the grain is a smaller serpentine vein that pinches out as its axis curves upwards and away from the trace of $(001)_{Fo}$. Two $(010)_{Fo}$-parallel high-Z veinlets are also present, and a serpentine vein terminates against each. e) A grain that contains a single $(001)_{Fo}$-parallel serpentine vein with serrated walls. The vein fill has a high-Z axial band. At the base of the image, this vein terminates against a $(010)_{Fo}$-parallel high-Z veinlet. At the top of the image, the axial band of the serpentine vein extends into the mesostasis as a narrow curving vein and joins with the high-Z veinlet at the base of the grain. f) Bright-field TEM image of a foil (C1-foil A) that was cut from the grain in (e) (the midplane of the foil is labeled "FIB" in [e]). The axial band, which is black in this image owing to attenuation of electrons by the high-Z phyllosilicates, lies at an angle of 54° to the polished grain surface. As the pole to $(001)_{Fo}$ is inclined at 55° to the polished surface of the grain (see the pole figure in [e]), the true orientation of the vein axis is parallel to $(001)_{Fo}$. Flanking phyllosilicates are more finely crystalline and lower Z, although contain two narrow and discontinuous higher Z bands.

are typically less than 10 μm along their longest dimension, and in grains whose polished surface is close to $(010)_{CEN}$, their walls are parallel to the traces of $(100)_{CEN}$ and $(001)_{CEN}$, and so have the shape of a parallelogram (the angle between $(100)_{CEN}$ and $(001)_{CEN}$ is 108°) (Figs. 5c and 5d). The irregular patches of phyllosilicate tend to be larger, and although their shape is not as precisely crystallographically controlled, in any one grain, the straight edges of their walls tend to have a similar

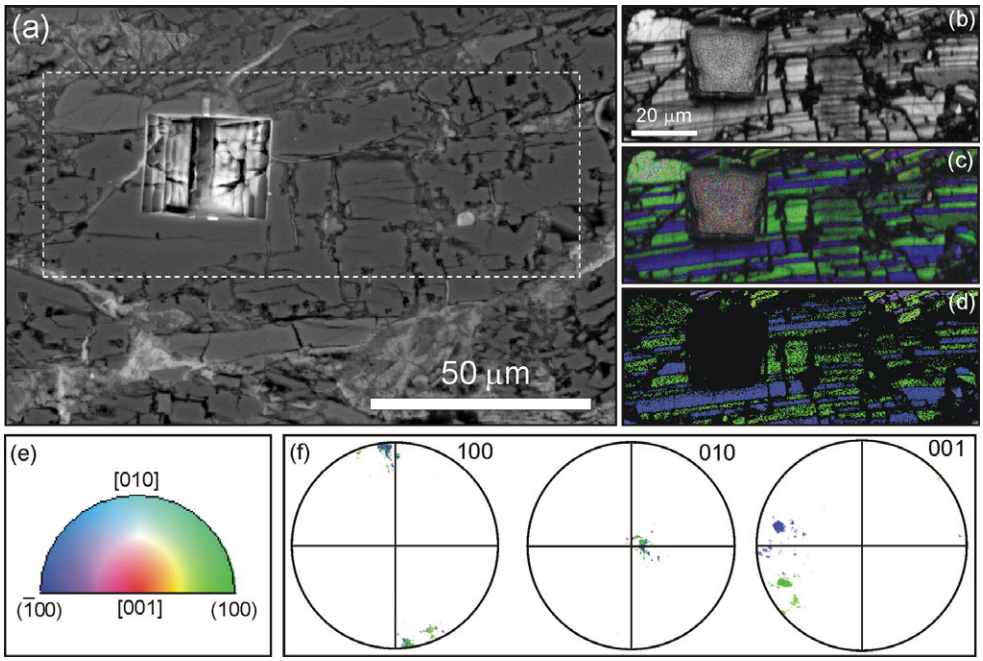

Fig. 4. a) BSE image of clinoenstatite in chondrule 3. The square pit marks the place from where C3-foil A was extracted. (b)–(d) EBSD maps obtained from the area that is outlined by the dashed white line in (a). b) Unprocessed image quality map containing 82608 points that were collected at a step size of 250 nm. The parallel bands with different image quality are $(100)_{CEN}$ twins. c) Inverse pole figure map overlain on the image quality map. The twins are different in color and so crystallographic orientation. d) Inverse pole figure map that has been processed by removal of data points with an image quality of less than 0.3, leaving 24% of the original points remaining. Many of the low image quality points correspond to the FIB-produced pit, and the phyllosilicate veins and patches. e) Diagram that describes the color scheme used to represent the crystallographic data. The colors in (c), (d), and (f) are expressed relative to a reference direction that is vertical compared to the images and pole figures as printed. Thus, the colors identify the poles that are oriented vertically; for example, the light green color in (c) and (d) indicates that the pole to $(100)_{CEN}$ is approximately vertical and in the plane of the page. f) Pole figures constructed using the data in (d) and with the same color coding. They show that the polished surface of the clinoenstatite grain is near-parallel to $(010)_{CEN}$, the twin composition planes are parallel to the trace of $(100)_{CEN}$, and most of the veinlets in (a) are oriented approximately parallel to the trace of $(001)_{CEN}$.

orientation (Figs. 7a and 7b). Arrays of slot-shaped pores that are very narrow (~30 nm in width) and short (<~1 μm) extend parallel to the trace of $(100)_{CEN}$ from the $(001)_{CEN}$-parallel walls of veinlets and patches. These pores can be resolved in BSE images (Figs. 5c and 5d), but are clearer in TEM foils where they give the walls of the patches a comb-like appearance (Fig. 7d).

Patches are distinguished from veinlets by their fill, which comprises loosely packed spherical or hemispherical low-Z particles whose diameter ranges from ~250 to 750 nm (Figs. 5c, 5d, 6a, 6b, and 7). Their elemental compositions are dominated by O, Mg, and Si, with low concentrations of Fe (Fig. 6d). TEM shows that the particles have a sectored internal structure and ~0.76 nm lattice fringe spacing (Figs. 7e and 7f). These properties are very similar to those of spherulites and sectored crystals of "Povlen-type" chrysotile that were described from the matrices of the Nawapali and Cochabamba CM carbonaceous chondrites by Barber (1981). In a TEM study of the matrices and fine-grained rims of the CMs Murchison, Mighei, and Cold Bokkeveld, Zega et al. (2006) also found tens to hundreds of nanometer-sized spherical crystals of serpentine with a sectored internal structure. They called these crystals "polyhedral serpentine," and this term is used here. Some of the polyhedral serpentine crystals in Murchison chondrules are in contact with clinoenstatite, but there is no evidence that they have formed by its replacement (which for example would be recognized by the interface between the serpentine and clinopyroxene following the curve of the rim of the polyhedral crystal) (Fig. 7d). Wavy laths of serpentine ~2 μm in length sometimes occur between the polyhedral crystals, and spatial relationships between the two types of serpentine suggest that the polyhedral crystals have nucleated on the laths (Fig. 7e). Barber (1981) also found that the "Povlen" spherulites in CM matrices had grown on plate-like phyllosilicate precursors.

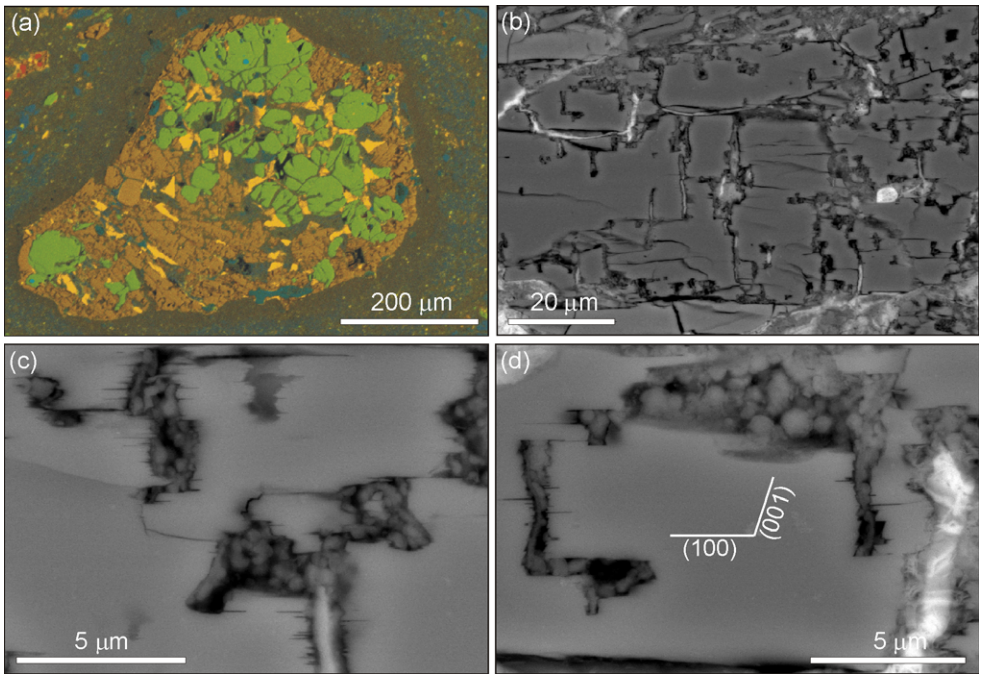

Fig. 5. Images of chondrule 3 and its partially serpentinized clinoenstatite grains. a) False color X-ray map of the chondrule, which is enclosed by a fine-grained rim. The elements included in the map are Si (red), Mg (green), Fe (blue), and Ca (yellow). Blending of these colors renders forsterite green, clinoenstatite brown, and augite yellow (note that the color blending is different to that used for chondrule 1 in Fig. 3b). b) BSE image of a clinoenstatite grain displaying the characteristic "skeletal" microstructure, which is due to abundant veinlets and patches of phyllosilicate. EBSD shows that the polished surface of this grain lies close to $(010)_{CEN}$. (c) and (d) are BSE images of parts of the clinoenstatite grain in (b). $(100)_{CEN}$ is horizontal and $(001)_{CEN}$ is inclined at 108°; both planes lie at 90° to the polished grain surface. The patches contain loosely packed submicrometer-sized spherical/hemispherical grains of polyhedral serpentine, whereas veinlets have a fill with a substantially higher Z. Note the very narrow pores that extend into clinoenstatite and parallel to (100) from the edges of patches and veins.

DISCUSSION

This study has sought new insights into the aqueous alteration of the Murchison parent body, which is most likely a C-complex asteroid. The focus of our work is on forsterite and clinoenstatite, and for two reasons (1) these minerals are together the dominant constituents of type IAB chondrules, which are the most abundant chondrules in Murchison (Bouvier et al. 2013); (2) forsterite and clinoenstatite are similar in chemical composition (i.e., Mg-silicate) but differ in crystal structure and microstructure, and so can potentially reveal the influence of intracrystalline properties on water–mineral interaction. Before interpreting results from our study of the forsterite and clinoenstatite, previous work on aqueous alteration of Murchison is reviewed.

Evidence for Parent Body Aqueous Alteration of Murchison

Phyllosilicates were tentatively identified in Murchison by Lovering and Le Maitre (1971) and were described in detail by Fuchs et al. (1973). These minerals are interpreted by most workers to be the products of aqueous alteration in the CM parent body(ies) (e.g., Barber 1981; Richardson 1981; Johnson and Prinz 1993; Brearley et al. 1999; Benedix et al. 2003; Howard et al. 2009, 2011; Lee et al. 2014). The aqueous solutions are believed to have been circum-neutral to alkaline and mildly reducing (Zolensky et al. 1989; Guo and Eiler 2007). Alteration temperatures of 0–25 °C have been calculated by assuming that Murchison phyllosilicates formed along with carbonates and in equilibrium with a common fluid reservoir (Clayton and Mayeda 1984, 1999), whereas Guo and Eiler (2007) used the clumped isotope thermometer to determine that Murchison calcite had precipitated at 20–33 °C. The question of whether Murchison and other CM carbonaceous chondrites were altered by aqueous fluids that were essentially static or had flowed through the parent body has been debated at length (e.g., Young et al. 1999; Bland et al. 2009). While the presence of a calcite vein in the CM carbonaceous chondrite Lonewolf Nunataks 94101 provides evidence for localized fluid flow through fractures (Lindgren et al.

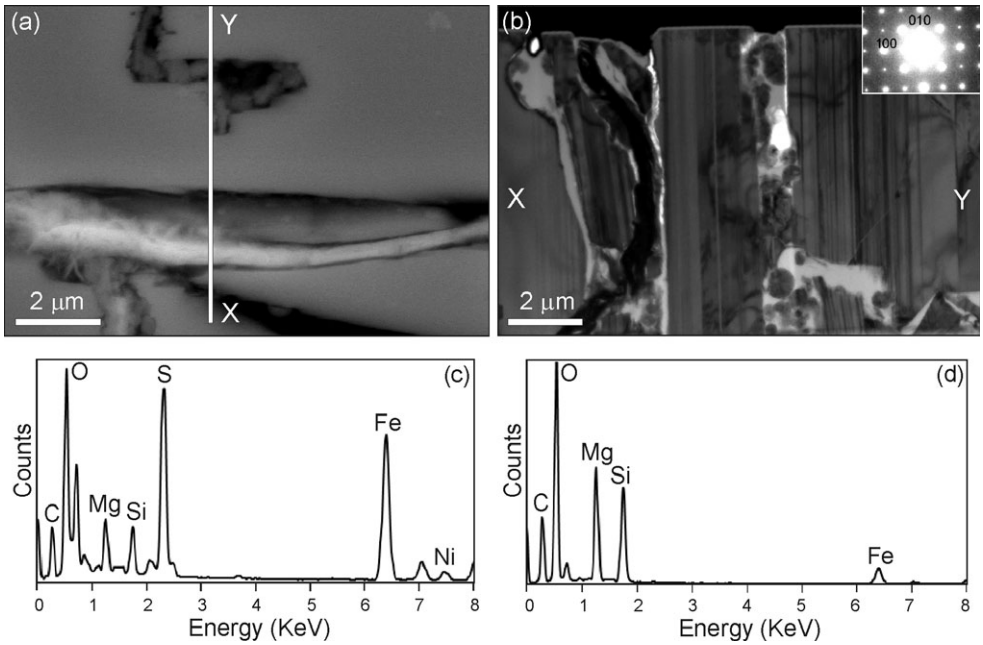

Fig. 6. Images of the clinoenstatite grain in Fig. 5. a) BSE image of the part of the grain that was studied by TEM. The high-Z phyllosilicate vein is oriented parallel to the trace of $(100)_{CEN}$ and contains small fibers on its left-hand side (just above the scale bar). The upper phyllosilicate patch has sections parallel to the traces of $(100)_{CEN}$ and ~$(001)_{CEN}$, as determined by EBSD, and contains crystals of polyhedral serpentine. b) Bright-field TEM image of a foil (C3-foil A) whose midplane is delineated by the line X–Y in (a). A corresponding $[001]_{CEN}$ SAED pattern is inset. The parallel and straight lines are orthopyroxene lamellae and twin composition planes. The high-Z vein is sinuous and black (due to attenuation of electrons, not scattering). In the uppermost ~4 μm of the foil, the walls of the polyhedral serpentine patch are parallel to the trace of $(100)_{CEN}$, then the patch widens toward the base of the foil. Individual crystals of polyhedral serpentine are difficult to resolve at this magnification. The light gray areas are resin-filled pores, the white areas are holes, and the black band along the top edge of the image is the Pt strap. (c) and (d) are LV-STEM X-ray spectra of the high-Z vein and a polyhedral serpentine crystal, respectively.

2011; Lee et al. 2013a, 2013b), the very low permeability of carbonaceous chondrite matrices would have inhibited the intergranular movement of aqueous solutions (Bland et al. 2009).

Evidence for alteration of Murchison chondrules was first described by Fuchs et al. (1973). They found that the chondrule mesostasis is composed of serpentine, including berthierine, and coined the term "spinach" for these phyllosilicates on account of their green color when viewed in thin section using plane polarized transmitted light. Fuchs et al. (1973) concluded that the spinach had formed by reaction of mesostasis glass with a nebula gas, but subsequent studies have established that the chondrules were altered by aqueous fluids and in a parent body environment (Richardson and McSween 1978; Richardson 1981). Chemical analysis of chondrule mesostasis in Murchison, and in other CMs including Y 791198, ALH 81002, and QUE 97990, has confirmed that serpentine is its main constituent (Brearley et al. 1999; Hanowski and Brearley 2001; Maeda et al. 2009). The mesostasis of CM chondrules is assumed to have originally been composed of glass, and this inference has recently been supported by the discovery of a type IIA chondrule with an unaltered mesostasis in the mildly altered CM EET 96029 (Lindgren and Lee 2015). In addition to glass, the EET 96029 mesostasis contains quench crystallites of Ca-rich pyroxene and grains of Fe-sulfide and Fe, Ni metal. Its composition is dominated by SiO_2 (~55 wt%), Al_2O_3 (~14 wt%), CaO (~11 wt%), and FeO (~10 wt%). To replace mesostasis of such a chemical composition by serpentine would have required, at a minimum, the import of Mg and export of Al and Ca, presumably by diffusional exchange with solutions hosted within the chondrule and enclosing matrix (Zega and Buseck 2003).

Despite evidence in the present study for serpentinization of forsterite and clinopyroxene, Rubin et al. (2007) found that silicate mineral phenocrysts in Murchison chondrules appear to have been unaffected by alteration. Velbel et al. (2015) placed Murchison in stage 1 of a seven-stage scheme for describing the aqueous processing of CM carbonaceous chondrites, where stage 0 is least altered and stage 6 is most highly processed (this is an extension of a four-stage scheme for chondrule alteration that was devised by Hanowski

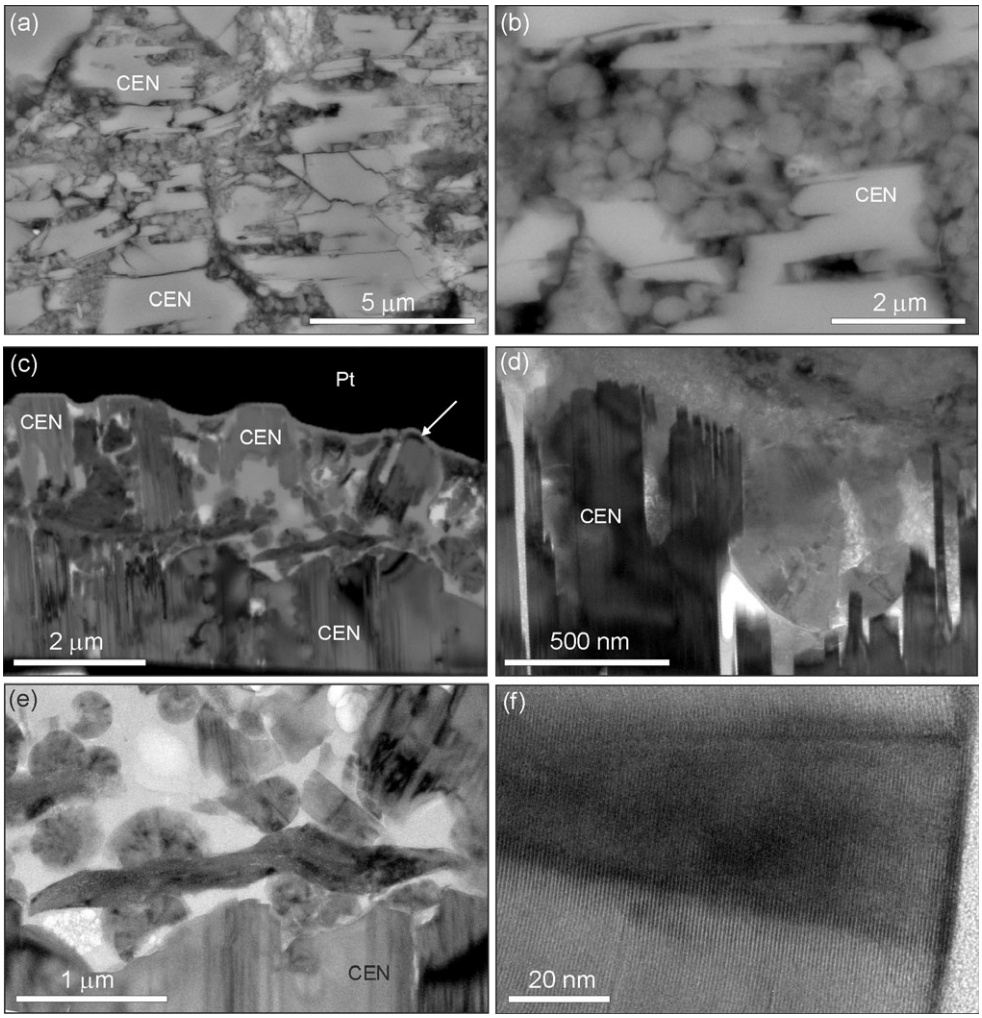

Fig. 7. Images of irregular patches of serpentine within a clinoenstatite grain (CEN) from chondrule 3. (a) and (b) are BSE images of patches that contain polyhedral serpentine. c–e) Bright-field TEM images of a foil that was cut from an irregular patch (C3-foil B). c) The upper part of the foil contains ragged shards of clinoenstatite, two of which are labeled, and the right-hand shard (arrowed) has been rotated relative to the others. The lower part of the foil contains intact clinoenstatite. Between the shards and intact clinoenstatite are crystals of polyhedral and lath-shaped serpentine that are surrounded by epoxy resin (light gray). The lower region of clinoenstatite grain was oriented with the electron beam parallel to $[011]_{CEN}$ so that the trace of $(100)_{CEN}$ is vertical (SAED pattern not shown). FIB-deposited platinum (Pt) is on the upper edge of the foil (i.e., the former surface of the polished block). d) The left-hand part of the foil in (c), showing the comb-like interface between clinoenstatite (black owing to strong electron scattering) and phyllosilicate; a crystal of polyhedral serpentine is near to the middle of the image. e) The interface between intact clinoenstatite and the area of phyllosilicate, which contains both polyhedral and lath-shaped crystals. Note that some of the polyhedral serpentine crystals have nucleated on the wavy lath. f) High-resolution TEM image of sectors within a polyhedral serpentine crystal. The lattice fringes have a spacing of ~0.76 nm.

and Brearley 2001). It was assumed by Velbel et al. (2015) that forsteritic olivine in Murchison chondrules is pristine, and serpentinization of coarse-grained olivine and clinopyroxene is seen only at advanced intermediate stages of CM alteration (i.e., at stage 3). The discrepancy between the previous work and results of this study could be accounted for if chondrules in the BM1970,5 (P19262) sample have been more highly altered than other parts of the meteorite. Our survey of four other polished blocks of Murchison has confirmed that forsterite phenocrysts in BM1970,5 (P19262) chondrules are somewhat more altered than in the other samples, but even in the least altered block, BM1988, M23 (P19261), four of the ten chondrules that were examined contain at least one partially serpentinized olivine phenocryst (Table 1). We, therefore, propose two reasons why aqueous alteration of Murchison forsterite and clinopyroxene grains has not been previously described (1) in at least some parts of the meteorite the serpentine veins and veinlets are quite

rare, and (2) the veinlets, veins, and patches are difficult to identify by SEM imaging owing to their small size and the limited difference in Z between most of the phyllosilicates and their host silicate minerals.

Serpentinization of Forsterite

Intragranular Controls on Alteration

The orientation preference of the veinlets and veins may help to reveal intragranular drivers of forsterite alteration. As EBSD has shown that the axes of serpentine veins in differently oriented forsterite grains all lie close to the trace of $(001)_{Fo}$ (e.g., compare the grains in Figs. 3c, 3d, and 3e), it is likely that $(001)_{Fo}$ is their true orientation. This assumption is consistent with results from the forsterite grain in Figs. 3e and 3f, which demonstrate that the axis of its serpentine vein is parallel to $(001)_{Fo}$ in three dimensions. Phyllosilicate veins oriented parallel to (001) have also been described from olivine grains in the ALH 81002 CM carbonaceous chondrite (Hanowski and Brearley 2001). The preferred orientation of veins in CM chondrule olivine has been interpreted to reflect a control on serpentinization by pre-existing fractures (Hanowski and Brearley 2001; Velbel et al. 2012, 2015). While we have found evidence that intragranular fractures were indeed present during serpentinization, for them to have controlled the formation of discontinuous veins, these fractures would need to have penetrated only a few tens of micrometers into the forsterite grains from their margins and parallel to (001) (e.g., Fig. 1b). It is equally possible that such discontinuous veins could have formed from sheet pores that were created by the crystallographically controlled congruent dissolution of forsterite that was propagating inwards from grain margins.

Comparison with Altered Olivine from Earth

Another approach to understanding the drivers of aqueous alteration of Murchison forsterite grains is to compare and contrast the textures of their veins with those of altered terrestrial olivine grains. Veins of iddingsite (a fine-scale intergrowth of smectite with Fe-oxides/hydroxides) within olivine from terrestrial basalts and basaltic andesites are typically oriented parallel to (001) (Baker and Haggerty 1967; Delvigne et al. 1979; Smith et al. 1987; Banfield et al. 1990). The walls of these veins also commonly have a "sawtooth" (i.e., serrated) microstructure (Baker and Haggerty 1967; Delvigne et al. 1979). These veins have clearly not formed by exploiting cleavage planes, which are on $(010)_{Fo}$ and $(100)_{Fo}$ (Deer et al. 1992). An explanation for their preferred orientation has been provided by Welch and Banfield (2002) who suggested that (001)-parallel channels in fayalite form by preferential protonation of cations on M1 sites. Velbel et al. (2012, 2015) noted that veins in olivine grains from CM carbonaceous chondrites lack serrated walls, thus suggesting a fundamental difference in the nature of water–olivine interaction between CM parent body interiors and the Earth's crust. However, our work has shown that serrations are commonplace on the walls of (001)-parallel veins in Murchison forsterite grains. One possible explanation for the discrepancy between findings of this study and previous work is that serrated walls of (001)-parallel veins will be seen only in those grains whose polished surface has a certain crystallographic orientation. Our results suggest that the teeth and notches have the three-dimensional shapes of ridges and valleys, respectively. The axes of these ridges and valleys are parallel to $[100]_{Fo}$ so that serrations will be seen in cross-section (i.e., will be most pronounced) only on those grains whose polished surfaces lie close to $(100)_{Fo}$ (i.e., at 90° to $[100]_{Fo}$). Conversely, serrations will be effectively invisible in those grains whose polished surfaces are parallel to $(010)_{Fo}$ (i.e., parallel to $[100]_{Fo}$). Thus, if multiple olivine grains were imaged whose polished surfaces were closer to $(010)_{Fo}$ than $(100)_{Fo}$, the serrations would indeed be much less prominent or apparently absent.

Comparison with Altered Olivine from Mars

Iddingsite veins in olivine phenocrysts ($\sim Fo_{30}$) from the nakhlite (Martian) meteorites have the same crystallographic orientation as veins in terrestrial and CM olivines (i.e., their axes are parallel to (001)) (Lee et al. 2013a, 2013b, 2015a, 2015b; Tomkinson et al. 2013). Many of these nakhlite veins are discontinuous and extend only a few tens of micrometers into olivine grains from their margins. There is good petrographic evidence that this iddingsite formed by interface-coupled dissolution–precipitation (Tomkinson et al. 2013), and in the Lafayette meteorite, the propagation of veins into grain interiors was guided by low-angle subgrain boundaries on (001), which may have formed by shock. Olivine grains in the Nakhla and Lafayette nakhlites also contain screw dislocations with a [001] Burgers vector, at a density of $\sim 10^8$ cm^{-2} (Lee et al. 2013a, 2013b, 2015a; Tomkinson et al. 2013). These defects could have controlled the development of teeth and notches on retreating (001)-parallel vein walls by localizing points of high solubility, which would have developed into the apices of the notches (Lee et al. 2013a, 2013b). In an attempt to assess whether defects had a comparable control on the development of serpentine veins in Murchison forsterite, a foil was extracted from just beyond the tip of the discontinuous vein in Fig. 1b. Results show that the forsterite is free

of subgrain boundaries and other defects (i.e., it has a dislocation density of $<10^6$ cm^{-2}), which is consistent with the lower shock stage of Murchison than the nakhlites (i.e., S1 versus S2–S3, respectively). Thus, there is no evidence that dislocations or subgrain boundaries controlled or influenced the serpentinization of Murchison forsterite.

This comparison of aqueously altered olivine from three very different regions of the solar system shows that the crystallographic controls on water–mineral interaction are very similar despite significant contrasts in the chemical composition and microstructure of the olivine and parent body history. The preferential development of veins parallel to (001) is ultimately due to the anisotropy in solubility of olivine (i.e., olivine dissolves most rapidly parallel to [001]), which is likely to reflect the nature of bonding within the olivine crystal structure, although more work is required in order to confirm this conclusion.

Sequence of Veinlet and Vein Formation

Aqueous alteration of Murchison forsterite started with the formation of submicrometer wide selvages of Fe-rich serpentine to create a network of veinlets. These high-Z phyllosilicates are the sole fill of the $(010)_{Fo}$ veinlets and form the axial band of the $(001)_{Fo}$ veins (this axial band is equivalent to the "central parting" described from within Nogoya and QUE 93005 serpentine veins by Velbel et al. 2012, 2015). Given the relatively high concentration of S and Fe in the fill of these veinlets, they are likely to have formed during alteration of chondrule Fe, Ni metal and Fe-sulfide. Hanowski and Brearley (1997, 2001) found that cronstedtite had formed during early stages of alteration of olivine in LEW 90500 and ALH 81002 (both CMs), and this mineral could also occur on the axes of Murchison veins. The S in Murchison olivine-hosted veinlets may be in tochilinite layers within the cronstedtite, although none was identified by SAED or high-resolution TEM imaging. As the high-Z selvages can be traced from veinlets into the enclosing mesostasis (e.g., Fig. 3e), their formation may have been linked to the influx of a fluid different from the one that was responsible for aqueous alteration of the original glass.

Veins of finely crystalline Mg-Fe serpentine formed after the high-Z phyllosilicates and by replacement of forsterite; the same sequence of mineralization (i.e., cronstedtite followed by microcrystalline Mg-Fe serpentine) was described from LEW 90500 olivine-hosted veins by Hanowski and Brearley (1997). In Murchison chondrules, this replacement reaction was most rapid parallel to $[001]_{Fo}$ and so most effective on those vein walls that were oriented close to $(001)_{Fo}$. The clearest evidence that the serpentine veins were widened by replacement rather than by filling of open pores is the serrated boundaries between bands, which represent the former interfaces between advancing serpentine and retreating serrated vein walls. At the same time as the veins were being widened, those grain margins that were oriented parallel to $(001)_{Fo}$ were being altered to form the centripetal replacement shells. Browning et al. (2000) described narrow (<~10 μm) rims of fine-grained phyllosilicates surrounding olivine grains within chondrules from CM meteorites and likewise interpreted them to have formed by replacement.

Using chemical analyses of olivine-hosted serpentine veins in Nogoya and QUE 93005 chondrules, Velbel et al. (2012, 2015) concluded that replacement is isovolumetric. As a consequence of these volume constraints, the replacement of forsterite results in export of Mg and Si from the vein and import of Fe. Velbel et al. (2012) suggested that the reactions in Nogoya had taken place on time scales in the subyear to decadal range. If contrasts between CMs in their degree of alteration correspond to differences in the duration of water–mineral reaction, rather that water/rock ratio or temperature, then the serpentine veins in Murchison, which is significantly less altered than Nogoya, will have formed over an even shorter time scale.

Serpentinization of Clinoenstatite

Veinlet Formation

The textures of partially serpentinized clinoenstatite grains have some similarities but also marked differences to those of forsterite grains in the same chondrules. The clinoenstatite-hosted veinlets have a compact fill of high-Z phyllosilicates whose chemical composition and d-spacings are indicative of tochilinite. In common with those in forsterite, the clinoenstatite-hosted veinlets are interpreted to have formed early and probably toward the end of mesostasis alteration. Hanowski and Brearley (1997, 2001) likewise concluded that the first phase of clinoenstatite alteration in type IAB chondrules from the CMs LEW 90500 and ALH 81002 was the formation of submicrometer wide veins. In LEW 90500, this fill comprises cronstedtite, whereas in ALH 81002, it is rich in Fe and contains 2–12 wt% S. Hanowski and Brearley (1997, 2001) suggested that some of the veins in both meteorites had formed within "contraction cracks" that were oriented normal to the *c* axis; Brearley (1997) likewise found that clinoenstatite in chondrules from Allende (CV3 carbonaceous chondrite) had been altered to amphibole and talc along contraction cracks. These cracks form by shortening of the *c* axis of protoenstatite (the high-temperature polymorph of $MgSiO_3$) accompanying its

transformation to clinoenstatite (the *c* axes of the two minerals differ by 2.8%) (Yasuda et al. 1983). In Y–74191 (a L3 ordinary chondrite), these contraction cracks are 0.05–0.5 μm in width (in Murchison they are 0.61–2.75 μm wide) and may be open or filled by glass (Yasuda et al. 1983). We therefore conclude that some or all of the (001)-parallel veinlets in Murchison clinoenstatite formed by tochilinite filling pre-existing contraction cracks.

Origin of the Rectilinear and Irregular Patches

A second generation of pores is interpreted to have formed within the clinoenstatite grains by congruent dissolution, which was guided by $(100)_{CEN}$ orthopyroxene lamellae, and possibly also by $(100)_{CEN}$ twin composition planes. Some of these pores were sufficiently large that shards of clinoenstatite have been displaced and rotated relative to their host grain (Fig. 7c). The influence of orthopyroxene lamellae on congruent dissolution is revealed most clearly by the comb-textured edges of veins (Figs. 5c and 5d) and patches (Fig. 7d). Hanowski and Brearley (2001, p. 511) also noted that (001)-parallel surfaces within ALH 81002 clinoenstatite grains have a "highly ragged and embayed appearance." The strong $(100)_{CEN}$ control on dissolution may be due to a concentration of elastic strain at the interfaces between orthopyroxene lamellae and their clinopyroxene host. The same microstructures have also guided the replacement of clinoenstatite in CM matrices by calcite (Lee et al. 2014). Textures produced by the congruent dissolution of Murchison clinoenstatite are very different to the denticulate features that characterize naturally weathered terrestrial pyroxenes (Velbel and Barker 2008; Velbel and Losiak 2010; Velbel 2011). The reasons for these contrasts are unknown, but they may be simply due to a difference in the scale and technique of observation (i.e., TEM in this study versus SEM in Velbel and Losiak 2010) or to mineralogical and microstructural differences, specifically the occurrence within Murchison of clinoenstatite (with orthopyroxene lamellae), which is very rare on Earth.

Origin of Polyhedral Serpentine

The rectilinear and irregular patches within Murchison clinoenstatite characteristically contain polyhedral serpentine, and three lines of evidence suggest that these crystals formed by the filling of pore spaces (1) the polyhedral crystals are loosely packed; (2) they have grown from the walls of veins and patches and the surfaces of serpentine laths; and (3) there is no evidence for replacement of clinoenstatite where it is in contact with the polyhedral crystals. This conclusion is consistent with observations of terrestrial serpentinites, which contain loosely packed spherical and hemispherical crystals of polyhedral serpentine that range in diameter from ~100 nm to several micrometers (Baronnet et al. 2007; Andreani et al. 2008). The crystallization of polyhedral serpentine on Earth is favored by the following conditions (1) an open space for the serpentine to grow into, and this space typically occurs within orthopyroxene (enstatite); (2) temperatures are <200–300 °C; and (3) incorporation of trivalent cations during serpentine crystal growth (i.e., Al^{3+}/Fe^{3+}) (Andreani et al. 2008). Our interpretation that polyhedral serpentine forms primarily by filling of pore spaces differs from Zega et al. (2006). They concluded that polyhedral serpentine in the matrices and fine-grained rims of CM carbonaceous chondrites is a product of aqueous alteration of cronstedtite (under oxidizing conditions) or glass. Our new evidence, therefore, suggests that the occurrence of polyhedral serpentine can be used to reveal the former location of pore spaces in meteorite matrices and fine-grained rims. Zega et al. (2006) found that polyhedral serpentine is the last in a sequence of serpentine minerals to form during progressive aqueous alteration of the CMs, and this conclusion is in good agreement with our observation that in Murchison chondrules it had formed after the tochilinite-bearing high-Z veinlets.

Implications for Understanding the Drivers of Parent Body Serpentinization

Results of this study have shown that the style of alteration of chondrule-hosted Mg-silicates varies over time, and in later stages, it is strongly dependent on their crystal structure and microstructure. The first generation of secondary minerals formed by the filling of narrow and elongate pores and these veinlets are broadly comparable in composition between forsterite and clinoenstatite (i.e., rich in S and Fe). We speculate that this secondary mineral chemistry reflects the tail-end of alteration of Fe, Ni metal and Fe-sulfides elsewhere within the chondrule. Forsterite was then replaced by finely crystalline serpentine, and fluctuations in solution chemistry produced a compositional banding. At around the same time, clinoenstatite grains underwent congruent dissolution, and the resulting pores were filled by crystals of polyhedral serpentine. The approximately equal degree of alteration of the two silicate minerals is notable given that the experimental dissolution rate of forsterite in acidic solutions is approximately an order of magnitude greater than that of enstatite (e.g., at pH5, 3.6×10^{-10} mol m^{-2} s^{-1} versus 3.2×10^{-11} mol m^{-2} s^{-1}, respectively; Brantley 2003). Evidence from this study suggests that the microstructure of chondrule clinoenstatite is responsible

for its elevated rate of reaction (i.e., high density of orthopyroxene lamellae and twin planes). Another contributing factor, as suggested by Hanowski and Brearley (2001), is probably the presence of intracrystalline fluid conduits created by the contraction cracks.

The differences in habit of serpentine crystals within forsterite and clinoenstatite may reflect contrasts in the space available for crystal growth (i.e., a very narrow solution film between retreating forsterite and centripetally expanding serpentine versus few micrometer-sized open pores within clinoenstatite). These space differences could in turn reflect contrasts in the relative rates of dissolution of the primary silicate minerals and precipitation of serpentine; for example, an equal rate of forsterite dissolution and serpentine mineral precipitation would allow the two reactions to be coupled at the mineral–fluid interface. Alternatively, the ratios of Si to Mg and Fe that were being liberated from the dissolving forsterite may have been more suitable for immediate precipitation of serpentine than the Mg and Si being liberated from reactive surfaces of clinoenstatite grains.

CONCLUSIONS

The evidence described here for multiphase alteration of forsterite and clinopyroxene within Murchison chondrules demonstrates that these Mg-rich silicate minerals have interacted with aqueous solutions at the earliest stages of CM parent body processing. The nature of water–rock interaction is strongly dependent on crystal structure and on microstructures developed during the cooling of chondrules from their high temperatures of formation within the solar nebula. Specific conclusions are as follows:

1. Alteration of the forsterite grains started with the formation of Fe-rich veinlets by filling of sheet pores oriented parallel to $(010)_{Fo}$ or $(001)_{Fo}$. These pores had formed by congruent dissolution and/or fracturing.
2. Those veinlets whose walls were parallel to $(001)_{Fo}$ were later widened by the centripetal replacement of forsterite by Mg-Fe serpentine. Fluctuations in fluid chemistry during replacement, in particular concentrations of S and Fe, produced a compositional banding.
3. The orientation of serpentine veins in forsterite crystals is crystallographically controlled so that veins will apparently be absent from most of those grains whose polished surface lies close to $(001)_{Fo}$. Serrated vein walls will be most pronounced in those grains whose polished surface is parallel to $(100)_{Fo}$, and absent from those grains whose polished surface is parallel to $(010)_{Fo}$.
4. Similarities in the crystallographic orientation and microstructure of secondary mineral veins between Murchison chondrule olivine, and olivine from the crusts of Earth and Mars, show that its aqueous alteration is controlled primarily by its crystal structure.
5. The first stage of clinoenstatite alteration is marked by the formation of high-Z veinlets, most of which were produced by the filling of cracks that had been generated by the transformation of protoenstatite to clinoenstatite.
6. Clinoenstatite subsequently underwent congruent dissolution that was guided by $(100)_{CEN}$ orthopyroxene lamellae and possibly also by $(100)_{CEN}$ twin composition planes. The resulting pore spaces were filled by submicrometer-sized spherical/hemispherical crystals of polyhedral serpentine.
7. The formation of polyhedral serpentine crystals both in terrestrial serpentinites and in CM carbonaceous chondrite parent bodies is genetically linked to the presence of pore spaces, especially those formed by the congruent dissolution of pyroxene.

Acknowledgments—We thank Caroline Smith (Natural History Museum, London) for loan of the Murchison samples and Peter Chung, William Smith, and Colin How (University of Glasgow) for assistance with the SEM, FIB, and TEM, respectively. We are also grateful to Laurence Garvie, Michael A. Velbel, and Adrian Brearley for their detailed and helpful reviews. This work was funded by the UK Science and Technology Facilities Council through grants ST/H002960/1, ST/K000942/1, and ST/L002167/1.

Editorial Handling—Dr. Adrian Brearley

REFERENCES

Alexander C. M. O'D., Howard K. T., Bowden R., and Fogel M. L. 2013. The classification of CM and CR chondrites using bulk H, C and N abundances and isotopic compositions. *Geochimica et Cosmochimica Acta* 123:244–260.

Andreani M., Grauby O., Baronnet A., and Muñoz M. 2008. Occurrence, composition and growth of polyhedral serpentine. *European Journal of Mineralogy* 20:159–171.

Baker I. and Haggerty S. E. 1967. The alteration of olivine in basaltic and associated lavas. Part II: Intermediate and low temperature alteration. *Contributions to Mineralogy and Petrology* 16:258–273.

Banfield J. F., Veblen D. R., and Jones B. F. 1990. Transmission electron-microscopy of subsolidus oxidation

and weathering of olivine. *Contributions to Mineralogy and Petrology* 106:110–123.

Barber D. J. 1981. Matrix phyllosilicates and associated minerals in C2M carbonaceous chondrites. *Geochimica et Cosmochimica Acta* 45:945–970.

Barber D. J. 1985. Phyllosilicates and other layer-structured materials in stony meteorites. *Clay Minerals* 20:415–454.

Baronnet A., Andréani M., Grauby O., Devouard B., Nitsche S., and Chaudanson D. 2007. Onion morphology and microstructure of polyhedral serpentine. *American Mineralogist* 92:687–690.

Benedix G. K., Leshin L. A., Farquhar J., Jackson T., and Thiemens M. H. 2003. Carbonates in CM2 chondrites: Constraints on alteration conditions from oxygen isotopic compositions and petrographic observations. *Geochimica et Cosmochimica Acta* 67:1577–1588.

Bland P. A., Jackson M. D., Coker R. F., Cohen B. A., Webber J. B. W., Lee M. R., Duffy C. M., Chater R. J., Ardakani M. G., McPhail D. S., McComb D. W., and Benedix G. K. 2009. Why aqueous alteration in asteroids was isochemical: High porosity $\neq$ high permeability. *Earth and Planetary Science Letters* 287:559–568.

Bouvier A., Wadhwa M., Simon S. B., and Grossman L. 2013. Magnesium isotopic fractionation in chondrules from the Murchison and Murray CM2 carbonaceous chondrites. *Meteoritics & Planetary Science* 48:339–353.

Brantley S. L. 2003. Reaction kinetics of primary rock-forming minerals under ambient conditions. In *Treatise on geochemistry, Vol. 5: Surface and ground water, weathering, and soils*, edited by Drever J. I. Amsterdam: Elsevier. pp. 73–117.

Brearley A. J. 1997. Disordered biopyriboles, amphibole, and talc inthe Allende meteorite: Products of nebular or parent body aqueous alteration? *Science* 276:1103–1105.

Brearley A. J. and Hutcheon I. D. 2002. Carbonates in the Y 791198 CM2 chondrite: Zoning and Mn-Cr systematics (abstract). *Meteoritics & Planetary Science* 37:A23.

Brearley A. J., Hanowski N. P., and Whalen J. F. 1999. Fine-grained rims in CM carbonaceous chondrites: A comparison of rims in Murchison and ALH 81002 (abstract #1460). 30th Lunar and Planetary Science Conference. CD-ROM.

Browning L. B., McSween H. Y. Jr, and Zolensky M. E. 1996. Correlated alteration effects in CM carbonaceous chondrites. *Geochimica et Cosmochimica Acta* 60:2621–2633.

Browning L. B., McSween H. Y. Jr, and Zolensky M. E. 2000. On the origin of rim textures surrounding anhydrous silicate grains in CM carbonaceous chondrites. *Meteoritics & Planetary Science* 35:1015–1023.

Bunch T. E. and Chang S. 1980. Carbonaceous chondrites—II. Carbonaceous chondrite phyllosilicates and light element geochemistry as indicators of parent body processes and surface conditions. *Geochimica et Cosmochimica Acta* 44:1543–1577.

Chizmadia L. J. and Brearley A. J. 2008. Mineralogy, aqueous alteration, and primitive textural characteristics of fine-grained rims in the Y-791198 CMS carbonaceous chondrite: TEM observations and comparison to ALHA81002. *Geochimica et Cosmochimica Acta* 72:602–625.

Clayton R. N. and Mayeda T. K. 1984. The oxygen isotope record in Murchison and other carbonaceous chondrites. *Earth and Planetary Science Letters* 67:151–166.

Clayton R. N. and Mayeda T. K. 1999. Oxygen isotope studies of carbonaceous chondrites. *Geochimica et Cosmochimica Acta* 63:2089–2104.

De Leuw S., Rubin A. E., Schmitt A. K., and Wasson J. T. 2009. ^{53}Mn–^{53}Cr systematics of carbonates in CM chondrites: Implications for the timing and duration of aqueous alteration. *Geochimica et Cosmochimica Acta* 73:7433–7442.

Deer W. A., Howie R. A., and Zussman J. 1992. *An introduction to the rock-forming minerals*, 2nd edn. London: Longman Scientific & Technical. 696 p.

Delvigne J., Bisdom E. B. A., Sleeman J., and Stoops G. 1979. Olivines: Their pseudomorphs and secondary products. *Pedologie* 39:247–309.

DuFresne E. R. and Anders E. 1962. On the chemical evolution of the carbonaceous chondrites. *Geochimica et Cosmochimica Acta* 26:1085–1114.

Endress M., Zinner E., and Bischoff A. 1996. Early aqueous activity on primitive meteorite parent bodies. *Nature* 379:701–703.

Fuchs L. H., Olsen E., and Jensen K. J. 1973. Mineralogy, mineral-chemistry, and composition of the Murchison (C2) meteorite. *Smithsonian Contributions to Earth Science* 10:39.

Fujiya W., Sugiura N., Hotta H., Ichimura K., and Sano Y. 2012. Evidence for the late formation of hydrous asteroids from young meteoritic carbonates. *Nature Communications* 3:627.

Graham A. L., Bevan A. W. R., and Hutchison R. 1985. *Catalogue of meteorites*. Tucson, Arizona: University of Arizona Press.

Greenwood R. C., Lee M. R., Hutchison R., and Barber D. J. 1994. Formation and alteration of CAIs in Cold Bokkeveld (CM2). *Geochimica et Cosmochimica Acta* 58:1913–1935.

Guo W. and Eiler J. M. 2007. Temperatures of aqueous alteration and evidence for methane generation on the parent bodies of CM chondrites. *Geochimica et Cosmochimica Acta* 71:5565–5575.

Hanna R. D., Ketcham R. A., and Hamilton V. E. 2012. Inclusion foliation in Murchison as revealed by high resolution X-ray CT (abstract #1242). 43rd Lunar and Planetary Science Conference. CD-ROM.

Hanowski N. P. and Brearley A. J. 1997. TEM observations of advanced silicate alteration in chondrules of the CM carbonaceous chondrite, LEW 90500 (abstract). *Meteoritics & Planetary Science* 32:A56.

Hanowski N. P. and Brearley A. J. 2001. Aqueous alteration of chondrules in the CM carbonaceous chondrite, Allan Hills 81002: Implications for parent body alteration. *Geochimica et Cosmochimica Acta* 65:495–518.

Hewins R. H., Bourot-Denise M., Zanda B., Leroux H., Barrat J-A., Humayun M., Göpel C., Greenwood R. C., Franchi I. A., Pont S., Lorand J.-P., Cournéde C., Gattacceca J., Rochette P., Kuga M., Marrocchi Y., and Marty B. 2014. The Paris meteorite, the least altered CM chondrite so far. *Geochimica et Cosmochimica Acta* 124:190–222.

Howard K. T., Benedix G. K., Bland P. A., and Cressey G. 2009. Modal mineralogy of CM2 chondrites by X-ray diffraction(PSD-XRD). Part 1: Total phyllosilicate abundance and the degree of aqueous alteration. *Geochimica et Cosmochimica Acta* 73:4576–4589.

Howard K. T., Benedix G. K., Bland P. A., and Cressey G. 2011. Modal mineralogy of CM2 chondrites by X-ray diffraction (PSD-XRD). Part 2: Degree, nature and settings of aqueousalteration. *Geochimica et Cosmochimica Acta* 75:2735–2751.

Howard K. T., Alexander C. M. O'D., Schrader D. L., and Dyl K. A. 2015. Classification of hydrous meteorites (CR, CM and C2 ungrouped) by phyllosilicate fraction: PSD-XRD modal mineralogy and planetesimal environments. *Geochimica et Cosmochimica Acta* 149:206–222.

Hutcheon I. D., Weisberg M. K., Phinney D. L., Zolensky M. E., Prinz M., and Ivanov A. V. 1999. Radiogenic ^{53}Cr in Kaidun carbonates: Evidence for very early aqueous activity (abstract #1722). 30th Lunar and Planetary Science Conference. CD-ROM.

Johnson C. A. and Prinz M. 1993. Carbonate compositions in CM and CI chondrites, and implications for aqueous alteration. *Geochimica et Cosmochimica Acta* 57:2843–2852.

Lee M. R. and Greenwood R. C. 1994. Alteration of calcium- and aluminium-rich inclusions (CAIs) in the Murray (CM2) carbonaceous chondrite. *Meteoritics* 29:780–790.

Lee M. R. and Smith C. L. 2006. Scanning transmission electron microscopy using a SEM: Applications to mineralogy and petrology. *Mineralogical Magazine* 70:561–572.

Lee M. R., Bland P. A., and Graham G. 2003. Preparation of TEM samples by focused ion beam (FIB) techniques: Applications to the study of clays and phyllosilicates in meteorites. *Mineralogical Magazine* 67:581–592.

Lee M. R., Lindgren P., Sofe M. R., Alexander C. M. O'D., and Wang J. 2012. Extended chronologies of aqueous alteration in the CM2 carbonaceous chondrites: Evidence from carbonates in Queen Alexandra Range 93005. *Geochimica et Cosmochimica Acta* 92:148–169.

Lee M. R., Sofe M. R., Lindgren P., Starkey N. A., and Franchi I. A. 2013a. The oxygen isotope evolution of parent body aqueous solutions as recorded by multiple carbonate generations in the Lonewolf Nunataks 94101 CM2 carbonaceous chondrite. *Geochimica et Cosmochimica Acta* 121:452–466.

Lee M. R., Tomkinson T., Mark D. F., Stuart F. M., and Smith C. L. 2013b. Evidence for silicate dissolution on Mars from the Nakhla meteorite. *Meteoritics & Planetary Science* 48:224–240.

Lee M. R., Lindgren P., and Sofe M. R. 2014. Aragonite, breunnerite, calcite and dolomite in the CM carbonaceous chondrites: High fidelity recorders of progressive parent body aqueous alteration. *Geochimica et Cosmochimica Acta* 144:126–156.

Lee M. R., Tomkinson T., Hallis L. J., and Mark D. F. 2015a. Formation of iddingsite veins in the Martian crust by centripetal replacement of olivine: Evidence from the nakhlite meteorite Lafayette. *Geochimica et Cosmochimica Acta* 154:49–65.

Lee M. R., MacLaren I., Andersson S. M. L., Kovacs A., Tomkinson T., Mark D. F., and Smith C. L. 2015b. Opal-A in the Nakhla meteorite: A tracer of ephemeral liquid water in the Amazonian crust of Mars. *Meteoritics & Planetary Science* 50:1362–1377.

Lindgren P. and Lee M. R. 2015. Tracking the earliest stages of aqueous alteration in the mildly altered CM chondrite EET 96029 (abstract #1760). 46th Lunar and Planetary Science Conference. CD-ROM.

Lindgren P., Lee M. R., Sofe M. R., and Burchell M. J. 2011. Microstructure of calcite in the CM2 carbonaceous chondrite LON 94101: Implications for deformation history during and/or after aqueous alteration. *Earth and Planetary Science Letters* 306:289–298.

Lindgren P., Hanna R. D., Dobson K. J., Tomkinson T., and Lee M. R. 2015. The paradox between low shock-stage and evidence for compaction in CM carbonaceous chondrites explained by multiple low-intensity impacts. *Geochimica et Cosmochimica Acta* 148:159–178.

Lovering J. F. and Le Maitre R. W. 1971. Murchison C2 carbonaceous chondrite and its inorganic composition. *Nature Physical Science* 230:18–20.

Mackinnon I. D. R. and Zolensky M. E. 1984. Proposed structures for poorly characterized phases in C2M carbonaceous chondrite meteorites. *Nature* 309:240–242.

Maeda M., Tomeoka K., and Seto Y. 2009. Early aqueous alteration processes in the QUE 97990 and Y 791198 CM carbonaceous chondrites. *Journal of Mineralogical and Petrological Sciences* 104:92–96.

McSween H. Y. Jr. 1979. Alteration in CM carbonaceous chondrites inferred from modal and chemical variations in matrix. *Geochimica et Cosmochimica Acta* 43:1761–1770.

Ohashi Y. 1984. Polysynthetically-twinned structures of enstatite and wollastonite. *Physics and Chemistry of Minerals* 10:217–229.

Olsen A. A. and Rimstidt J. D. 2007. Using a mineral lifetime diagram to evaluate the persistence of olivine on Mars. *American Mineralogist* 92:598–602.

Richardson S. M. 1981. Alteration of mesostasis in chondrules and aggregates from three C2 carbonaceous chondrites. *Earth and Planetary Science Letters* 52:67–75.

Richardson S. M. and McSween H. Y. Jr. 1978. Textural evidence bearing on the origin of isolated olivine crystals in C2 carbonaceous chondrites. *Earth and Planetary Science Letters* 37:485–491.

Rubin A. E. 2012. Collisional facilitation of aqueous alteration of CM and CV carbonaceous chondrites. *Geochimica et Cosmochimica Acta* 90:181–194.

Rubin A. E., Trigo-Rodriguez J. M., Huber H., and Wasson J. T. 2007. Progressive alteration of CM carbonaceous chondrites. *Geochimica et Cosmochimica Acta* 71:2361–2382.

Scott E. R. D., Keil K., and Stöffler D. 1992. Shock metamorphism of carbonaceous chondrites. *Geochimica et Cosmochimica Acta* 56:4281–4293.

Smith K. L., Milnes A. R., and Eggleton R. A. 1987. Weathering of basalt: Formation of iddingsite. *Clays and Clay Minerals* 35:418–428.

Stopar J. D., Taylor G. J., Hamilton V. E., and Browning L. 2006. Kinetic model of olivine dissolution and extent of aqueous alteration on Mars. *Geochimica et Cosmochimica Acta* 70:6136–6152.

Tomeoka K. and Buseck P. R. 1985. Indicators of aqueous alteration in CM carbonaceous chondrites: Microtextures of a layered mineral containing Fe, S, O, and Ni. *Geochimica et Cosmochimica Acta* 49:2149–2163.

Tomeoka K., Yamahana Y., and Sekine T. 1999. Experimental shock metamorphism of the Murchison CM carbonaceous chondrite. *Geochimica et Cosmochimica Acta* 21:3683–3703.

Tomkinson T., Lee M. R., Mark D. F., and Smith C. L. 2013. Sequestration of Martian CO_2 by mineral carbonation. *Nature Communications* 4:2662.

Velbel M. A. 2009. Dissolution of olivine during natural weathering. *Geochimica et Cosmochimica Acta* 73:6098–6113.

Velbel M. A. 2011. Microdenticles on naturally weathered hornblende. *Applied Geochemistry* 26:1594–1596.

Velbel M. A. and Barker W. W. 2008. Pyroxene weathering to smectite: Conventional and low-voltage cryo-field emission scanning electron microscopy, Koua Bocca ultramafic complex, Ivory Coast. *Clays and Clay Minerals* 56:111–126.

Velbel M. A. and Losiak A. I. 2010. Denticles on chain silicate grain surfaces and their utility as indicators of weathering conditions on Earth and Mars. *Journal of Sedimentary Research* 80:771–780.

Velbel M. A., Tonui E. K., and Zolensky M. E. 2012. Replacement of olivine by serpentine in the carbonaceous chondrite Nogoya (CM2). *Geochimica et Cosmochimica Acta* 87:117–135.

Velbel M. A., Tonui E. K., and Zolensky M. E. 2015. Replacement of olivine by serpentine in the Queen Alexandra Range 93005 carbonaceous chondrite (CM2): Reactant–product compositional relations, and isovolumetric constraints on reaction stoichiometry and elemental mobility during aqueous alteration. *Geochimica et Cosmochimica Acta* 148:402–425.

Welch S. A. and Banfield J. F. 2002. Modification of olivine surface morphology and reactivity by microbial activity during chemical weathering. *Geochimica et Cosmochimica Acta* 66:213–221.

Yasuda M., Kitamura M., and Morimoto N. 1983. Electron microscopy of clinoenstatite from a boninite and a chondrite. *Physics and Chemistry of Minerals* 9:192–196.

Young E. D., Ash R. D., England P., and Rumble D. III. 1999. Fluid flow in chondritic parent bodies: Deciphering the compositions of planetesimals. *Science* 286:1331–1335.

Zega T. and Buseck P. R. 2003. Fine-grained-rim mineralogy of the Cold Bokkeveld CM chondrite. *Geochimica et Cosmochimica Acta* 67:1711–1721.

Zega T., Garvie L. A. J., Dodony I., Friedrich H., Stroud R. M., and Buseck P. R. 2006. Polyhedral serpentine grains in CM chondrites. *Meteoritics & Planetary Science* 41:681–688.

Zolensky M. E., Bourcier W. L., and Gooding J. L. 1989. Aqueous alteration on the hydrated asteroids: Results of EQ3/6computer simulations. *Icarus* 78:411–425.

Zolensky M. E., Barrett R., and Browning L. 1993. Mineralogy and composition of matrix and chondrule rims in carbonaceous chondrites. *Geochimica et Cosmochimica Acta* 57:3123–3148.

Zolensky M. E., Mittlefehldt D. W., Lipschutz M. E., Wang M.-S., Clayton R. N., Mayeda T. K., Grady M. M., Pillinger C., and Barber D. 1997. CM chondrites exhibit the complete petrologic range from type 2 to 1. *Geochimica et Cosmochimica Acta* 61:5099–5115.